Fabrication of graphene-covered micro-tubes for process intensification

J. Y. Chong[1,a], B. Wang[1], P. C. Sherrell[2], F. M. Pesci[2], C. Mattevi[2], K. Li[1,*]*

[1]Dr. J.Y. Chong, Dr. B. Wang, Prof. K. Li
Barrer Centre, Department of Chemical Engineering, Imperial College London, London SW7 2AZ, UK
E-mail: kang.li@imperial.ac.uk or bo.wang2@imperial.ac.uk

[2]Dr. P.C. Sherrell, Dr. F.M. Pesci, Dr. C. Mattevi
Department of Materials, Imperial College London, London SW7 2AZ, UK

[a]Dr. J.Y. Chong
Current address: Singapore Membrane Technology Centre, Nanyang Technological University, 1 Cleantech Loop, Singapore 637141

Keywords: graphene, CVD, micro-tube, phase inversion, copper

Abstract: Graphene is known for its high surface-area-to-mass ratio. However, for graphene to be used in engineering processes such as catalytic reactors or heat exchangers, high surface-area-to-volume ratio is essential. Currently, graphene is only prepared in sheet form, which limits its surface-area-to-volume ratio to around 200 m^2/m^3. In this study, we propose and demonstrate a technique based on chemical vapour deposition (CVD) to realise graphene on a copper-based micro-tubular substrate to not only substantially increase its surface-area-to-volume ratio to a value over 2000 m^2/m^3, but also to eliminate maldistribution of flows commonly unavoidable in flat-sheet configurations. Our approach uses a dual-layer micro-tubular substrate fabricated by a phase-inversion facilitated co-extrusion technique. In the substrate, a thin copper outer layer is employed to enable the CVD growth of graphene, and an inner Cu-Fe layer is adopted to provide a strong mechanical support. Our study shows that this approach is feasible to produce graphene with a very high surface-area-to-volume ratio for possible practical applications in catalytic reactors or heat exchangers, though problems such as the inter-diffusion between the two metal layers and defects in graphene need to be further addressed. To the best of our knowledge, this study is the first attempt to prepare graphene with high surface-area-to-volume ratio by a CVD route.

Graphene is an ultimate thin two-dimensional material, which is composed of one layer of hexagonally-arranged carbon atoms. Besides its two-dimensionality and high specific surface area, graphene also has other remarkable properties such as its superior mechanical strength, excellent electronic and thermal conductivity, and outstanding chemical inertness. [1] Because of these properties, graphene has been intensively studied as protective barriers, electrodes and selective membranes. [2] Furthermore, pristine graphene can be doped with other elements, for example, nitrogen and oxygen, to introduce active sites. The activated graphene can be used directly as metal-free catalysts or an excellent support for catalytic nanoparticles. [3]

Several techniques for preparing graphene-based thin films are now readily available. Two of the most commonly used techniques are the multi-layer assembly of exfoliated graphene or graphene oxide from graphite [4] and chemical vapour deposition (CVD). [5] Micron-scale graphene or graphene oxide flakes can be easily synthesised from graphite through exfoliation. The flakes exfoliated can be subsequently assembled into multi-layer thin films using methods such as filtration or solvent evaporation. The advantages of this approach include low synthesis cost and high efficiency [6]. The films obtained are relatively thick compared to the ones produced by CVD, usually with a thickness of tens to hundreds of nanometres. However, serious performance instabilities due to the change in microstructure have been widely noticed in these thin films [4b, 7]. On the other hand, CVD is used to grow continuous mono- or few-layer graphene films on a dense metal substrate, mainly copper foil or nickel foam. Such a method can achieve large area atom-level thin films without microstructural stability issues. Currently, the use of CVD to synthesise graphene thin films is limited to the flat-sheet configuration. [8]

However, for industrial applications, tubular shapes, especially micro-tubes, are highly favourable over flat-sheet configurations in many applications such as catalytic reactors and

heat exchangers, where graphene can play important roles as catalysts or a protective barrier. In these applications, factors such as the geometric area in unit volume, mass and heat transfer, or random distribution of flow, would severely reduce the performance of graphene-based systems. Flat-sheet configurations often need to use spacers to separate different elements, which usually limit the geometric area in a unit volume to 200 m^2/m^3. Furthermore, dead corners are easily formed in the flow passage in many flat-sheet configurations, and instable flow patterns could also be formed when two-phase or multi-phase flows are involved in the narrow gap between the flat sheets.[9] On the contrary, tubular geometries, especially micro-tubes, would allow a dense packing of tubular elements, thus achieve a very high area per unit volume, comfortably above 2000 m^2/m^3. Micro-tubular configurations also effectively eliminates dead corners and instable flow patterns, maximising the use of every tubular elements. In fact, tubular or micro-tubular designs have been widely used in industries, for example, heat exchanger, hollow fibre membranes, and honeycomb or monolith reactors to improve efficiency and reduce footprints. [10]

Here we demonstrate successful CVD growth of graphene on a copper-based dual-layer Cu/Cu-Fe micro-tubular substrate. In this micro-tubular substrate, a thin copper outer layer is made on top of the dual-phase Cu-Fe inner layer through our advanced co-extrusion/co-sintering technique [11]. The copper layer provides an active surface, on which the growth of graphene has been proven to be a reliable process. The iron-based inner layer gives tough mechanical property and reduces the use of more expensive copper. A portion of copper is blended into the iron matrix in the inner layer to enhance its adhesion with the outer copper layer, which could be critical for the stability of the layered structure when steep thermal gradients are applied repeatedly, for example in heat exchangers.

1. Experimental Section

1.1. Materials

Iron powder (99%, 1 - 3 μm, Alfa Aeser) and copper powder (0.5 - 1.5 μm, Sigma Aldrich) were used as supplied. Poly(methyl methacrylate) (PMMA) (average M_w ~120,000 by GPC, Sigma Aldrich) was used as the polymeric binder. N-methyl-2-pyrrolidone (NMP, HPLC grade, VWR) was used as the solvent. De-ionized water was used as the external and internal coagulants.

1.2. Fabrication of Cu/Cu-Fe Micro-tubular substrates

Dual-layer Cu/Cu-Fe micro-tubular substrates were fabricated through a phase-inversion/sintering process [10a, 11a, 12]. In this process, the metal powders were first mixed with PMMA and NMP to form a uniform suspension. The suspensions for the outer and inner layers were then extruded simultaneously through a triple-orifice spinneret. Meanwhile water was supplied through the central bore of the spinneret to the lumen of the nascent micro-tube. The nascent micro-tube then entered a water bath to go through the phase-inversion of the PMMA binder . The water bath acted as a coagulant to the PMMA binder, which extracted the solvent from the suspension and thus precipitated the PMMA. Schematics of the preparation setup are shown in ***Figure 1***, and the composition of the suspensions and fabrication parameters are given in ***Table 1***. The solidified PMMA bound the metal powder and created the micro-tubular geometry. The formed micro-tube was then transferred to a furnace for debinding to remove the organic materials at 500 °C, followed by sintering at 1000 °C to densify the micro-tubes, all in a H_2 atmosphere.

1.3. Growth of graphene films on the micro-tubular substrate by the CVD method

The CVD method for graphene film growth was via an adapted standard method using a vertical quartz tubular furnace [13]. The sintered micro-tubular substrate was heated to 1000 °C in H_2 for 15 minutes at a constant pressure of 5 torr. Then methane was introduced into the

furnace with a CH_4:H_2 ratio of 9:1 for 30 minutes. Finally the methane flow was stopped and the furnace was cooled down with a rate from 40 °C/min to 300 °C/min to get graphene films.

1.4. Characterisations

The morphologies and the elements of the micro-tube were characterized by using a scanning electron microscope (LEO Gemini 1525 FEGSEM and Zeiss Auriga Crossbeam). Raman spectrometry (WITec solid state, diode pumped 532 nm laser) was used to determine the quality of graphene synthesized. The mechanical strength of the micro-tube was evaluated by using an Instron material testing system (Model 5544) with a 10 kN load cell. A three-point bending method was used, where the samples were positioned onto a sample holder with a span of 40 mm.

2. Results and discussion

2.1. Cu/Cu-Fe micro-tubular substrates

Dual-layer Cu/Cu-Fe metallic micro-tubes were successfully fabricated using the phase-inversion facilitated co-extrusion/sintering approach. The suspension containing copper was used for the outer layer to form a continuous layer with a thickness of about 25 μm during the phase inversion. The Cu-Fe composite suspension was used for the inner layer that will provide support to the final micro-tube. The dual-layer structure of unsintered Cu/Cu-Fe micro-tube is clearly revealed in the optical microscope images in Figure 2a & b. The overall diameter of the unsintered micro-tube was around 2.1 mm. After phase inversion, the micro-tubes were fully sintered in hydrogen. The wall thickness of the micro-tube reduced from 270 μm to 230 μm after sintering with a linear shrinkage of 15 %. The outer diameter also reduced to 1.8 mm, which shall give an area to volume ratio of about 2200 m^2/m^3 at the modular level. The cross-section of the micro-tube showed a typical finger-like structure (Figure 2c), which was commonly seen in phase-inversion membranes, and the formation mechanism of such a

structure has been intensively discussed elsewhere [10a, 12, 14]. A more detailed observation at the boundary between the outer and inner layers (Figure 2d) revealed that the two layers were perfectly sintered together, and it was free of delamination or cracks. Figure 2d also shows that an apparent homogenous outer copper layer with a thickness of about 20 μm was obtained after sintering, while the inner layer presents a heterogeneous dual-phase structure. The well-sintered micro-tube showed very high mechanical strength with a three-point-bending fracture load of around 80 N with a 4 cm span, and can be bent to 90° without failure. The sintered micro-tube presents a shiny metallic copper surface, as shown in the inset of Figure 2e, indicating a smooth and dense surface structure. Indeed, the SEM image in Figure 2e shows that the surface was fully densified after sintering, and the boundaries between the large copper grains can be seen clearly. However, at higher magnifications in Figure 2f, intensive small features of sub-micron size are visible, suggesting the formation of a secondary phase on the copper surface. In fact, the small particles were not only found on the surface, but also in the bulk of the copper layer (Figure 2g). EDX mapping results confirmed that the secondary phase presented on the copper surface was iron (Figure 3). This can be attributed to the inter-diffusion between iron and copper at high temperature. Copper and iron are immiscible at low temperatures, [15] therefore iron diffused into the copper layer at high temperature would precipitate upon cooling and form small grains in copper due to a reduction in solubility at low temperature.

2.2. CVD results

Attempts to grow graphene on the Cu/Cu-Fe micro-tube by the CVD method have been made using the conditions typically for copper substrates [13]. Figures 4a and 4b show the SEM images of the micro-tube surface after the graphene growth. It was surprising that the surface morphology of the micro-tube changed after the CVD process and showed intensely dispersed

nodular (sample *a*) or branched (sample *b*) patterns, which were considerably different from the morphology after sintering but before CVD. EDX mapping results show that the nodules or branches are copper; and the iron phase on the samples before CVD, as shown in Figure 2, was not observed here. It is believed that the iron phase re-dissolved into the copper phase at the CVD temperature, but did not form again after CVD. The disappearance of the iron phase can be attributed to the fast cooling rate used in CVD, during which the diffusivity of iron in the copper phase reduces dramatically upon cooling, and the formation of the secondary iron phase was prohibited due to the slow kinetics. While the secondary iron phase could not be formed, periodical compositional fluctuation on surface could be generated during cooling [16]. At the same time, when copper vapour in the reactor at the high temperature condenses onto the micro-tube surface at lower temperatures, the deposition of copper vapour will be affected by the pattern of the compositional fluctuation, and the formation of patterns is possible. As the exact pattern is affected by the kinetics of both phase demixing and vapour deposition, it could be sensitive to various parameters such as vapour concentration and cooling rate, which may vary slightly at each operation, and thus the pattern could change for each trial.

To find more clues on the formation mechanism of the patterns, we reduced the copper vapour pressure during CVD by using a micro-tube that only has the inner layer. In this micro-tube, the majority of the surface exposed to the reactant gas was iron, and the copper content was reduced to 40 vol%. The surface after CVD showed those periodical patterns on neither the copper phase nor the iron phase, likely due to the reduced copper vapour pressure. Though it perhaps also related to the discontinuity of the copper phase on the surface, which disrupted the formation of the patterns, the result gives a good indication of the importance of copper vapour pressure. Unfortunately, a continuous graphene layer could not be obtained with this substrate due to the high content of iron on the surface. On the other hand, the patterned morphologies after the CVD process have not been reported on pure copper

substrates, indicating the importance of the presence of minor iron in the copper layer. At the moment, the formation mechanism of the patterns is still far from clear despite the speculations, and the exact reasons still need to be confirmed in the future.

The formation of the patterns on the surface does not seem to have affected the growth of graphene significantly. The characteristic G peak at 1600 cm^{-1} and 2D peak at 2700 cm^{-1} in Figure 4c imply the presence of graphene. Typically, a 2D to G peak intensity ratio of 2 is observed for a single-layer graphene and the ratio decreases when the number of graphene layer increases. A 2D/G ratio about 0.5 would indicate the presence of multi-layer graphene growth. In our case, mapping and distribution of the peak ratio in Figure 4d, e, f show a main distribution around 0.5, although some parts were covered by graphene of the ratio 2. The results indicate the presence of mainly multi-layer graphene together with small regions covered by single-layer graphene. There is also a minor peak at 1350 cm^{-1} in the Raman spectrums, particularly notable in the sample *a* shown in Figure 4c, which is the evidence of the existence of sp^3 carbon, ascribed typically to 5,7 ring defects and flake edges in the graphene [17]. These uncontrolled defects, while undesirable for potential applications when graphene acts as a protective barrier, present with a very low Raman intensity in our samples. Given the rough, complex geometry of the underlying substrate, the defect density is acceptable and is comparable to the best reported for graphene on 3D substrates [18]. Growth of graphene on 3D substrates will result in some defects due to compressive and tensile strain of the curved surface leading to smaller grain sizes, and sp^3 carbons to compensate for this strain during growth [19]. Furthermore, growing graphene on iron-based substrate is notoriously difficult, therefore it is reasonable to suspect that iron, and any dissolved carbon in the iron, could have a negative impact to the CVD process. For the sample *b* with the branched pattern, similar Raman spectroscopy results have also been obtained despite the very different surface morphology, but has a lower defect intensity than the sample *a*. The

graphene grown on this micro-tube is prominently multi-layer with improved homogeneity and slightly increased 2D:G ratio compared to the sample *a* (Figure 4d,f). This lower defect density and better homogeneity is hypothesised to arise due to the branched pattern on the sample *b*, enabling larger, more consistent graphene domains to grow. Regardless of the defects, growth of multi-layered graphene was successfully achieved on chemically complex, rough, micro-tubular substrates demonstrating the potential use of these systems for catalytic reactors or heat exchangers in the future.

3. Conclusions

In summary, dual-layer Cu/Cu-Fe micro-tube has been successfully fabricated. Although inter-diffusion between the outer and inner layers has been found to cause secondary phase formation in the outer copper layer under normal sintering conditions, it did not appear when a fast cooling rate was applied during the CVD graphene growth process. Graphene was successfully grown on the Cu/Cu-Fe micro-tube surface despite the notable surface morphological change, demonstrating the feasibility of preparing graphene thin films on this substrate. The micro-tubes would be useful in catalytic reactors as they can provide a high active area in a limited space. Besides, the graphene-protected copper-based micro-tube can be used in heat exchangers. Copper has very high thermal conductivity but is prone to corrosion under heat exchanger conditions; the protection from the graphene layer would ease the corrosion problem substantially and prolongs the service time in such a scenario.

Acknowledgements

The authors gratefully acknowledge the research funding provided by EPSRC in the United Kingdom (Grant no. EP/M022250/1).

Conflict of Interest

The authors declare no conflict of interest.

Received: ((will be filled in by the editorial staff))

Revised: ((will be filled in by the editorial staff))

Published online: ((will be filled in by the editorial staff))

References

[1] a) C. Lee, X. Wei, J. W. Kysar, J. Hone, *Science* **2008**, 321, 385; b) D. Prasai, J. C. Tuberquia, R. R. Harl, G. K. Jennings, K. I. Bolotin, *ACS Nano* **2012**, 6, 1102.

[2] a) K. Celebi, J. Buchheim, R. M. Wyss, A. Droudian, P. Gasser, I. Shorubalko, J.-I. Kye, C. Lee, H. G. Park, *Science* **2014**, 344, 289; b) M. J. Nine, M. A. Cole, D. N. H. Tran, D. Losic, *Journal of Materials Chemistry A* **2015**, 3, 12580; c) Y. Su, V. G. Kravets, S. L. Wong, J. Waters, A. K. Geim, R. R. Nair, *Nature Communications* **2014**, 5, 4843; d) C. Xu, B. Xu, Y. Gu, Z. Xiong, J. Sun, X. S. Zhao, *Energy & Environmental Science* **2013**, 6, 1388.

[3] a) D. Higgins, P. Zamani, A. Yu, Z. Chen, *Energy & Environmental Science* **2016**, 9, 357; b) Y. Li, H. Wang, L. Xie, Y. Liang, G. Hong, H. Dai, *J Am Chem Soc* **2011**, 133, 7296; c) H. Wang, T. Maiyalagan, X. Wang, *ACS Catalysis* **2012**, 2, 781.

[4] a) R. R. Nair, H. A. Wu, P. N. Jayaram, I. V. Grigorieva, A. K. Geim, *Science* **2012**, 335, 442; b) Y. Han, Z. Xu, C. Gao, *Advanced Functional Materials* **2013**, 23, 3693; c) N. F. D. Aba, J. Y. Chong, B. Wang, C. Mattevi, K. Li, *Journal of Membrane Science* **2015**, 484, 87.

[5] a) Y. Zhang, L. Zhang, C. Zhou, *Accounts of Chemical Research* **2013**, 46, 2329; b) X. Li, W. Cai, J. An, S. Kim, J. Nah, D. Yang, R. Piner, A. Velamakanni, I. Jung, E. Tutuc, S. K. Banerjee, L. Colombo, R. S. Ruoff, *Science* **2009**, 324, 1312; c) A. Reina, X. Jia, J. Ho, D. Nezich, H. Son, V. Bulovic, M. S. Dresselhaus, J. Kong, *Nano Letters* **2009**, 9, 30.

[6] Y. Wei, Y. Zhang, X. Gao, Z. Ma, X. Wang, C. Gao, *Carbon* **2018**, 139, 964.

[7] a) Y. Wei, Y. Zhang, X. Gao, Y. Yuan, B. Su, C. Gao, *Carbon* **2016**, 108, 568; b) J. Y. Chong, B. Wang, C. Mattevi, K. Li, *Journal of membrane science* **2018**, 549, 385.

[8] a) H. W. Kim, H. W. Yoon, S.-M. Yoon, B. M. Yoo, B. K. Ahn, Y. H. Cho, H. J. Shin, H. Yang, U. Paik, S. Kwon, J.-Y. Choi, H. B. Park, *Science* **2013**, 342, 91; b) S. C. O'Hern, C. A. Stewart, M. S. H. Boutilier, J.-C. Idrobo, S. Bhaviripudi, S. K. Das, J. Kong, T. Laoui, M. Atieh, R. Karnik, *ACS Nano* **2012**, 6, 10130.

[9] P. G. Saffman, *Journal of Fluid Mechanics* **2006**, 173, 73.

[10] a) K. Li, *Ceramic Membranes for Separation and Reaction*, Wiley, **2007**; b) M. van Bruijnsvoort, P. J. Schoenmakers, in *Encyclopedia of Separation Science*, DOI: https://doi.org/10.1016/B0-12-226770-2/05101-2 (Ed: I. D. Wilson), Academic Press, Oxford **2000**, p. 3312.

[11] a) J. Y. Chong, B. Wang, K. Li, *Journal of Membrane Science* **2017**, 541, 425; b) Z. Wu, B. Wang, K. Li, *Journal of membrane science* **2010**, 352, 63; c) Z. Wu, B. Wang, K. Li, *international journal of hydrogen energy* **2011**, 36, 5334.

[12] B. F. K. Kingsbury, K. Li, *Journal of Membrane Science* **2009**, 328, 134.

[13] C. Mattevi, H. Kim, M. Chhowalla, *Journal of Materials Chemistry* **2011**, 21, 3324.

[14] a) M. Lee, B. Wang, K. Li, *Journal of Membrane Science* **2016**, 503, 48; b) M. Lee, B. Wang, Z. Wu, K. Li, *Journal of membrane science* **2015**, 483, 1.

[15] M. Perez, F. Perrard, V. Massardier, X. Kleber, A. Deschamps, H. de Monestrol, P. Pareige, G. Covarel, *Philosophical Magazine* **2005**, 85, 2197.

[16] a) E. Quarez, K.-F. Hsu, R. Pcionek, N. Frangis, E. K. Polychroniadis, M. G. Kanatzidis, *Journal of the American Chemical Society* **2005**, 127, 9177; b) D. De Fontaine, N. E. Paton, J. C. Williams, *Acta Metallurgica* **1971**, 19, 1153.

[17] L. M. Malard, M. A. Pimenta, G. Dresselhaus, M. S. Dresselhaus, *Physics Reports* **2009**, 473, 51.

[18] J.-C. Yoon, J.-S. Lee, S.-I. Kim, K.-H. Kim, J.-H. Jang, *Scientific Reports* **2013**, 3, 1788.
[19] a) P. C. Sherrell, C. Mattevi, *Materials Today* **2016**, 19, 428; b) K. Chen, L. Shi, Y. Zhang, Z. Liu, *Chemical Society Reviews* **2018**, 47, 3018.

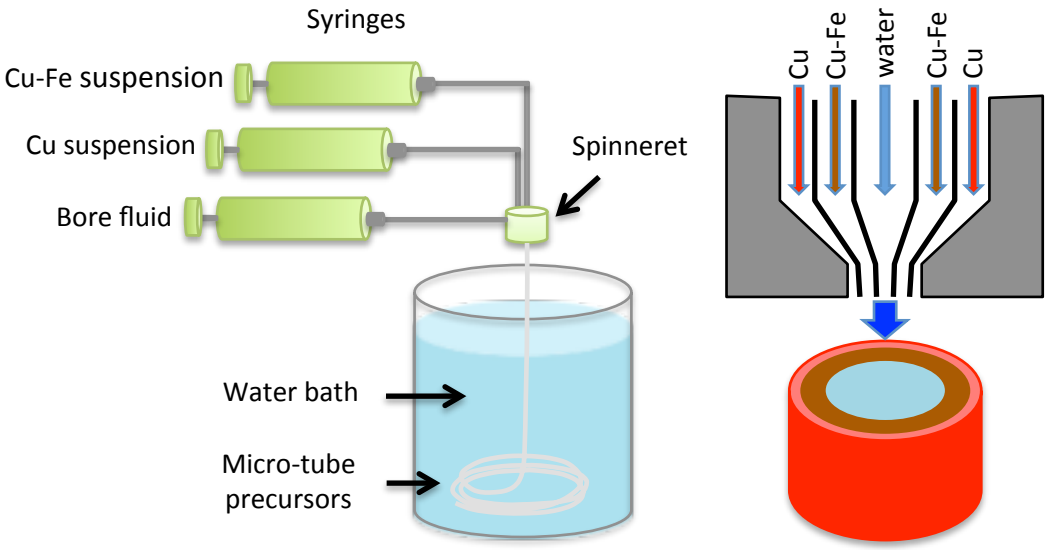

Figure 1. Schematics of the micro-tube preparation setup (left), the interior structure of the trible-orifice spinneret and the nascent micro-tube leaving the spinneret (right).

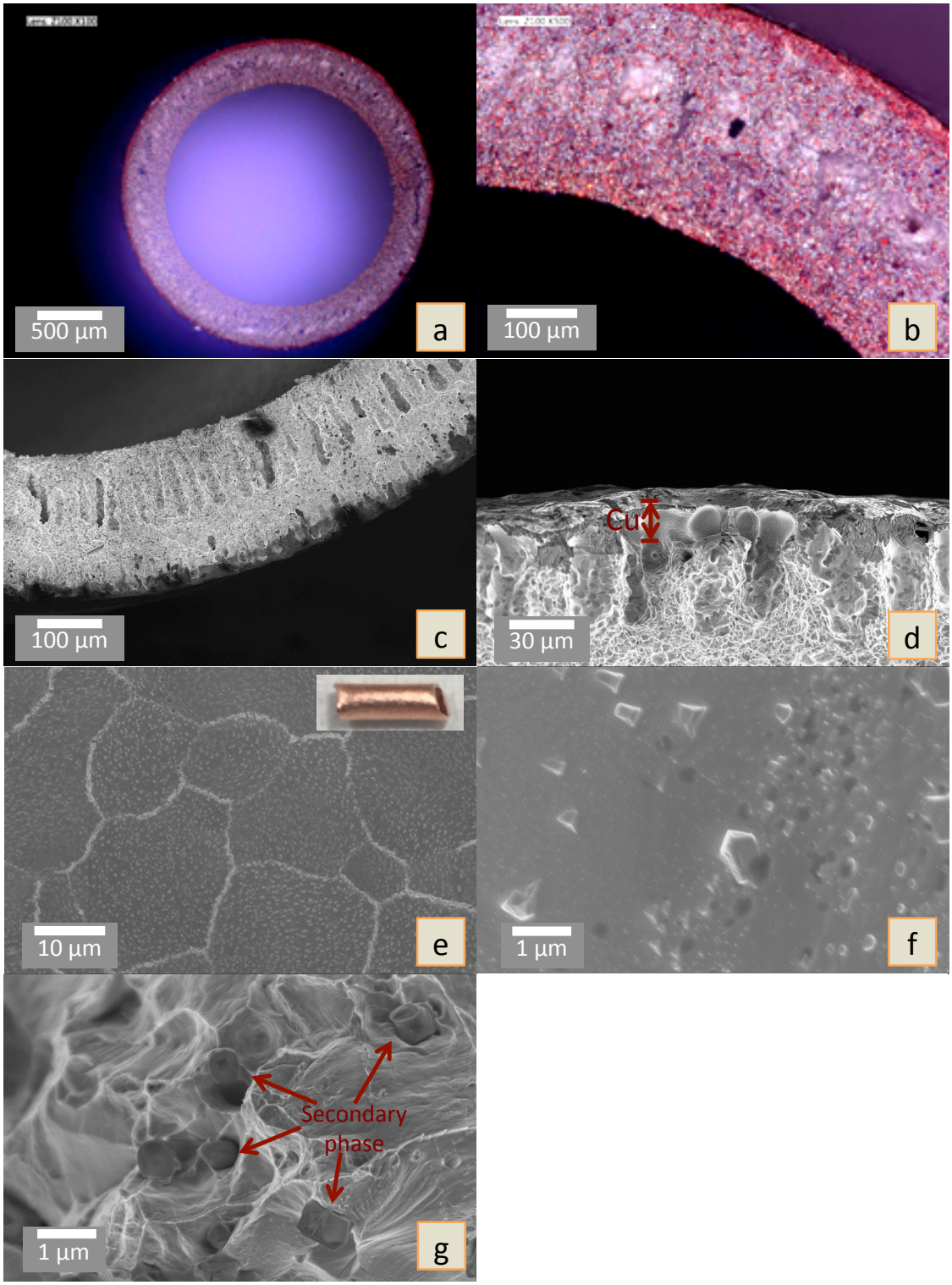

Figure 2. Morphologies of the Cu/Cu-Fe dual-layer micro-tube. (a) cross-sectional overview of the unsintered precursor, (b) cross section of the unsintered tube wall, (c) wall structure of the sintered micro-tube, (d) zoom-in image at the boundary between the inner and outer layers, which shows the copper layer thickness is 20 µm, (e) the outer surface of the sintered micro-tube, the inserted picture displays the appearance of the surface, (f) surface under higher magnification showing the existence of secondary-phase particles, (g) secondary-phase particles found in the bulk of the copper layer.

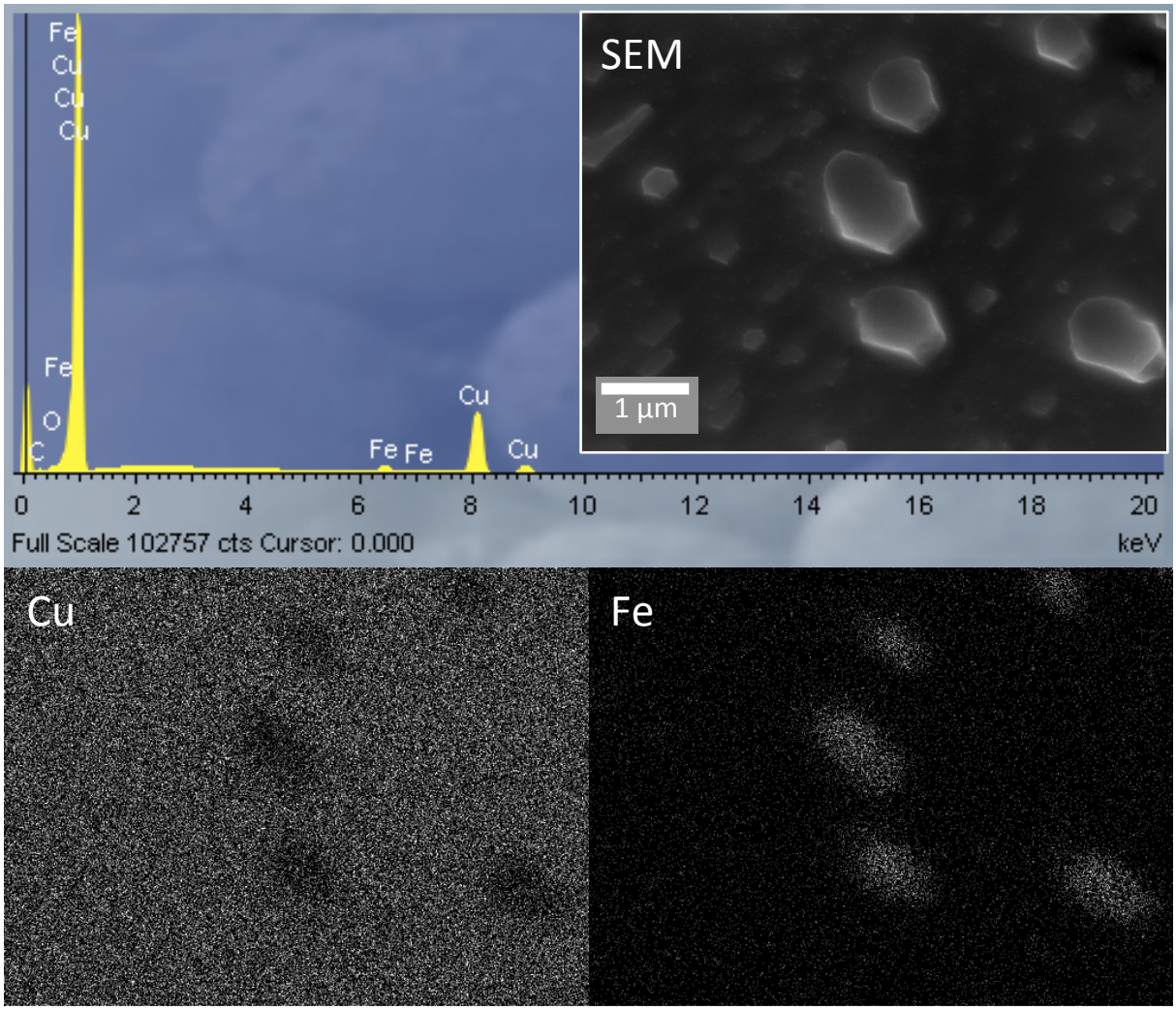

Figure 3. EDX mapping results on the surface of sintered Cu/Cu-Fe dual-layer micro-tube. The result shows clearly the second-phase particles give low copper signal and high iron signal.

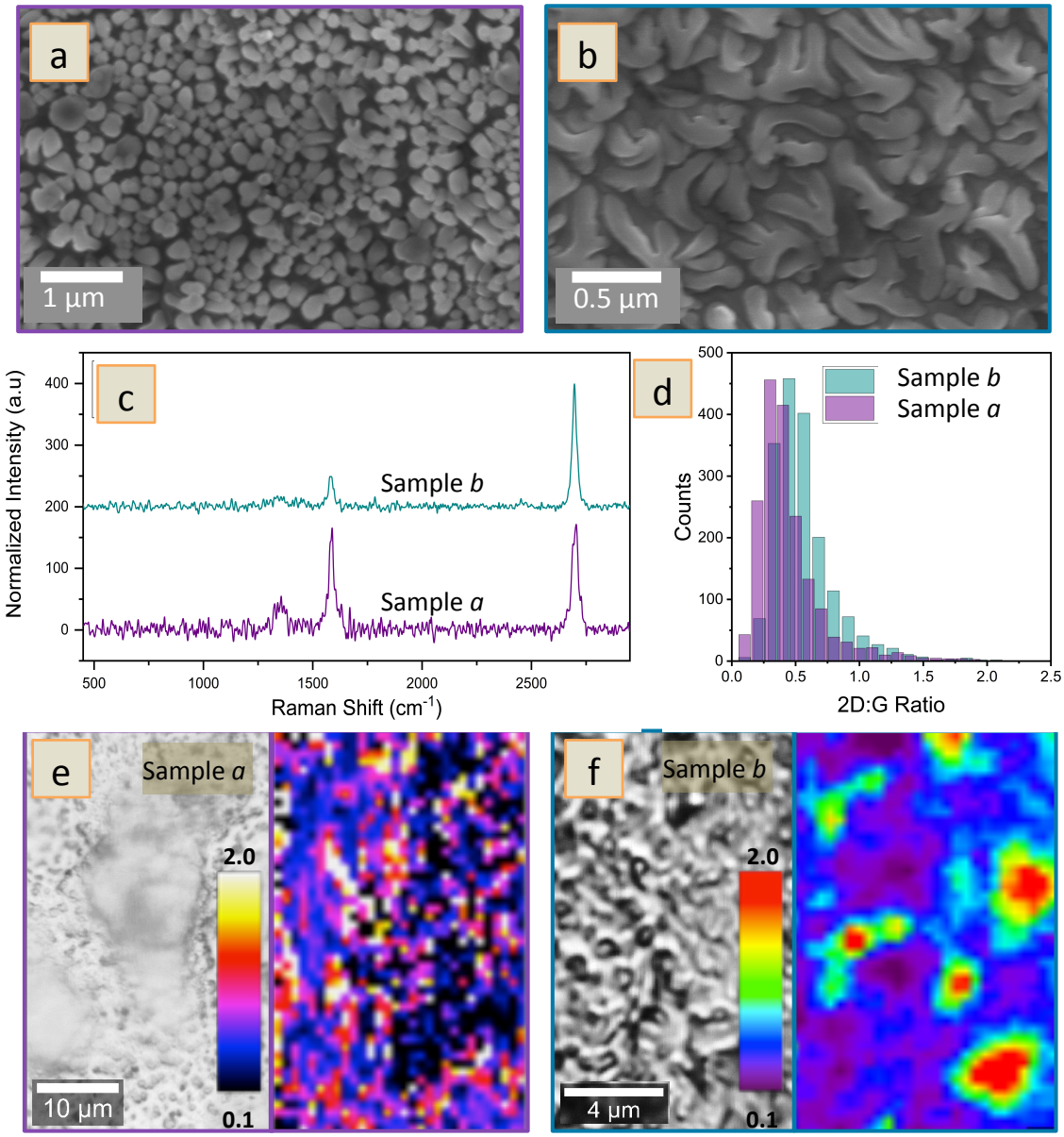

Figure 4. Two Cu/Cu-Fe micro-tube samples after CVD. Sample (a) shows a nodular surface structure while sample (b) shows a branched structure despite same CVD conditions were used for both samples. (c) representative Raman spectra of both samples; and (d) 2D:G histograms for the respective samples; (e,f) optical image and 2D:G Raman map of (a) and (b) respectively.

Table 1: Fabricating parameters of the Cu/Cu-Fe micro-tube

	Suspension composition (wt.%)	
	Cu suspension	Fe-Cu suspension
NMP	35.2	19
PMMA	8.5	5.7
Cu	56.3	32.5
Fe	-	42.8
Fabrication	Cu suspension extrusion rate (ml min^{-1})	2
	Cu-Fe suspension extrusion rate (ml min^{-1})	8
	Bore liquid rate (ml min^{-1})	30
	Air gap (cm)	15